SOUND RADIATION OF A SMOKE-REMOVAL FAN SYSTEM

Yann PASCO, Stéphane MOREAU

Université de Sherbrooke, Aeroacoustic Group, 2500 boulevard de l'Université, Sherbrooke, Qc, J1K2R1, Canada

SUMMARY

The aeroacoustics of a smoke-removal fan system used by firemen is studied. It consists in a 21" fan with straight blades and a classical constant tip clearance directly mounted on a thermal engine with a protecting grill upstream and a short volute downstream. Acoustic measurements have been done on the full system and without the grill and the volute. Scaling laws have been obtained to characterize the nature of the acoustic sources. Overall sound is found to be caused by two separate sources: a monopolar one mostly at low frequencies with significant tonal content caused by the thermal engine, and a dipolar one at mid and high frequencies with both tonal and broadband contributions caused by the fan system. A method to separate rotating and stationary noise sources has also been generalized and applied to yield the separate spectra of each noise source. The contribution of the different sound sources and of the different components of the system is also discussed depending on the operating condition.

INTRODUCTION

To remove toxic fumes from people caught in fire, firefighters use more and more powerful fan systems. These machines are designed to provide the maximum flow rate when the fire is the most intense. This ventilation power is directly connected with the problem of sound nuisances that interfere with the firefighter communications even if helmets are worn. The noise also causes premature fatigue for the firefighters. On a more long term, this sound nuisance (mainly the high-pitched tonal noise at the blade passing frequency and its harmonics) can trigger losses of hearing and eventually deafness, or other health hazards for the firefighters (increased heart diseases for instance). The present study is meant to provide details characterizations of the radiated sound of such systems and identify ways of reducing the associated noise.

A representative fire fan system has then been studied in the recently-built anechoic wind tunnel at Université de Sherbrooke at several operating conditions. Three different configurations have been studied and compared: the complete fan system, the fan system without the front grill, and the fan without front grill and volute. Detailed acoustic measurements have been achieved with a microphone directivity array that consists of 19 Bruel and Kjaer (B&K) microphones. The experimental set-up

and the different acoustic results are described in the next section. Scaling laws are also drawn from these data to yield the nature of sound sources. Finally having shown the main dipolar noise feature of sound of the fire fan system and the respective contribution of the thermal engine and the fan, a method to separate rotating and stationary noise sources has been successfully applied in the following section. The contribution of both noise components are then clearly identified, which allows a separate analysis of both noise sources. Conclusions are finally drawn and suggestions for future noise control are provided.

ACOUSTIC MESUREMENTS AND RESULTS

GF-210 fan system

The present smoke-removal fan system is the GF-210 model (see fig. 1) that consists of a thermic engine directly connected to a fan (observed in fig. 1 (b)). The engine is a 6 Hp Honda running from about 1440 Rounds Per Minute (RPM) at iddle to 3660 RPM at full speed. The fan itself is protected by a front and a rear grill, both attached to a volute. The fan tip clearance is more than 1 cm for safety purpose (see fig. 1(a)). The size of the fan is 21 inches in diameter. The fan has 7 straight blades. It can be tilted from 0 to 20 degrees to blow the air slightly upward. The main characteristics of the GF210 system is summarized in Tab. 1.

model	size	set back	angle (degree)	Airflow at free air (m^3/h)
GF210	21”	4’	20	24524
		6’	20	26547
		8’	20	29000
		10’	20	28548

Table 1: Technical specifications of the GF210 Fan. (www.euramcosafety.com)

Experimental set-up

The fan system is placed in the newly-built anechoic wind tunnel at Université de Sherbrooke [1]. Both far-field sound pressure spectra and directivities of all fan-system configurations in all engine regimes have been obtained with a microphone array placed in the meridional plane of the fan system. The microphone directivity array consists of 19 Bruel and Kjaer (B&K) microphones arranged in half a circle around the fan system as shown in Fig. 2.

The radius of the directivity antenna (see table 2) is 1.85 m and using this configuration, the sound pressure level radiating from the fan can be measured in the far field from radiation angles $\Theta = -90\,^\circ$ to +90 °, by increment of 10 ° (the fan axis being the reference as shown in Fig. 2).

radius	1.85m
resolution	10°
number of microphones	19 covering from -90 ° to 90 °

Table 2: Specifications of the directivity array

The fan was slightly tilted by 26 ° to avoid any trouble with the air flow impacting the front microphone located at zero degree.

(a) Front view (b) ISO view

Figure 1: GF210 fan system.

Sound spectra

The spectra of the far-field acoustic pressure or Sound Pressure Levels (SPL) for the complete system in front of the fan ($\Theta = 0\,^{\circ}$) are shown in Figs. 3 (a) and (b) at the full speed of 3600 RPM and the idle speed of 1440 RPM respectively. All spectra shown in this article are Power Spectral Densities (PSD) of the far-field acoustic pressure for a 1 Hz resolution with respect to a reference pressure of 2×10^{-5} Pa to yield dB/Hz. The PSD have been computed using 65536 points and Hanning windowing. The characteristics of these spectra is the superposition of several sources radiating in different ways with both tonal and broadband noise contributions. The high tonal noise with strongly emerging tones (more than 10 dB above the broadband noise) is most likely the main annoyance of this fan system. As shown below, it can be heard at all rotational speeds in all directions for all configurations. To help separate the sources in Figs. 3, the frequencies have been made dimensionless by the rotor Blade Passing Frequency (BPF).

The first source is the engine which is radiating with many harmonics at low frequencies (a full comb of tones emerging from the broad band noise up to about 2 BPF at full speed and 1.5 BPF at idle respectively). In Fig. 3(a) the fundamental engine frequency is close to 30 Hz which corresponds to a rotational speed of 3600 RPM divided by 2 because of the design of the engine (4-stroke). The radiated spectrum of the engine is then mainly a discrete tonal spectrum with a fundamental engine frequency, f_{motor}, of 30 Hz.

The second source is the fan. It first yields a tonal noise spectrum at the BPF. In the full engine regime, the first BPF is close to 420 Hz which corresponds to 7 times the rotational speed of 3600 RPM (60 Hz). The tonal part of the radiation of the fan is then a discrete spectrum of tones which frequencies are multiple of the BPF (420 Hz). The fan-noise radiation also has a broadband component. In Fig. 3 it can be seen as the black thick baseline on the spectrum.

At full speed, with all protections on (complete fan system), the noise is then essentially coming from the engine and the fan system. The tonal noise from the fan is usually coming from the interaction

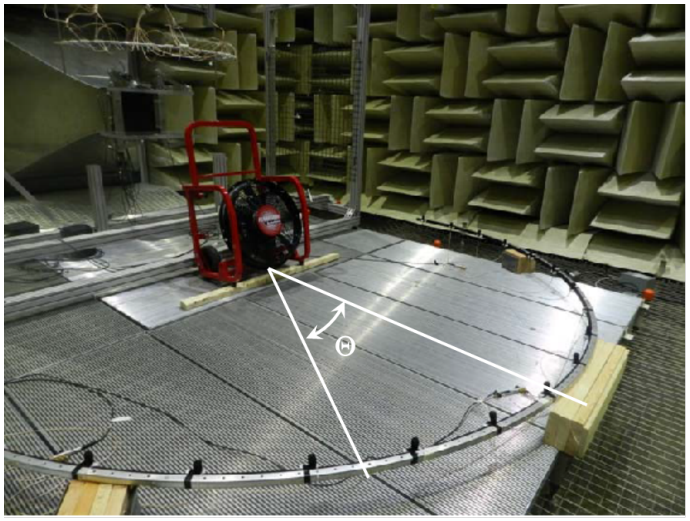

Figure 2: Setup of the 19 microphones for the directivity array.

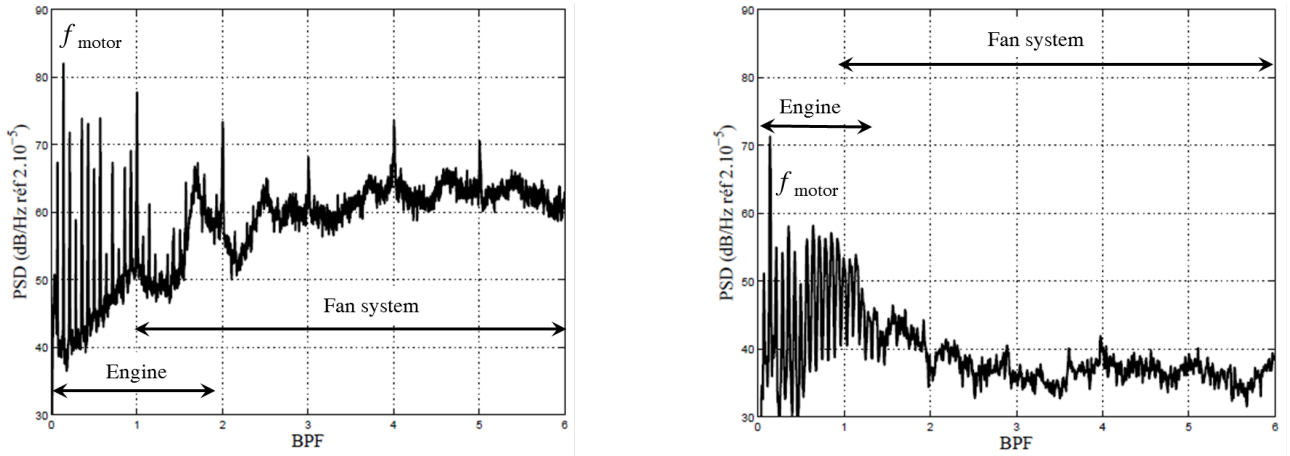

(a) Full speed (b) Idle speed

Figure 3: PSD of acoustic pressure at two engine regimes for the complete fan system ($\Theta = 0°$).

of the wake of the blade with fixed parts (like the protection front and back grills) and the broadband noise from the turbulent boundary layer growing on the fan blades (self-noise or Trailing-Edge Noise (TEN)), the tip clearance flow and the interaction of the impinging turbulent flow on the blade itself (Turbulence-Interaction Noise (TIN)) [2, 3, 4, 5].

The spectra for the other configurations without the front grill and without the front grill and volute are compared with the complete fan system in Figs. 4 at full speed (3660 RPM) and at $\Theta = 0\,°$. The spectra in Figs. 4 (a) and (b) have very similar shapes and levels. Therefore there is hardly any effect by removing the front grill. This means that there are no significant wake or potential effects due to the front grill. Removing both the front grill and the volute has however a strong effect on the broadband noise. Fig. 4 (c) shows a strong reduction by about 5 to 10 dB of the broadband noise over a large frequency range and particularly at mid frequencies. Only the subharmonic humps mostly caused by the tip flow and the coherent structures forming in the tip clearance keep the same levels and hardly shifted in frequency [5]. This might be a hint that the intense tip flow induced by the large tip gap is hardly modified in all configurations.

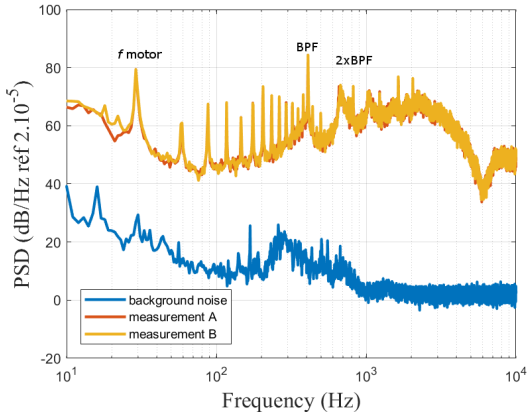

(a) Complete system

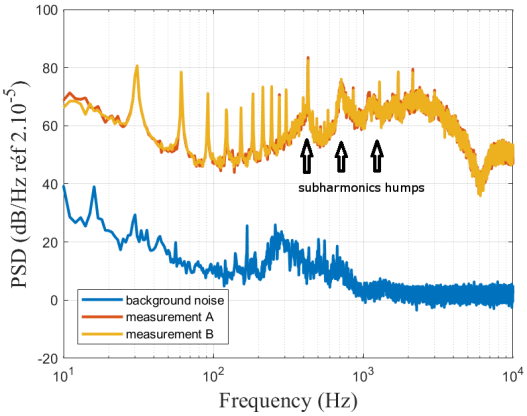

(b) System without front grill

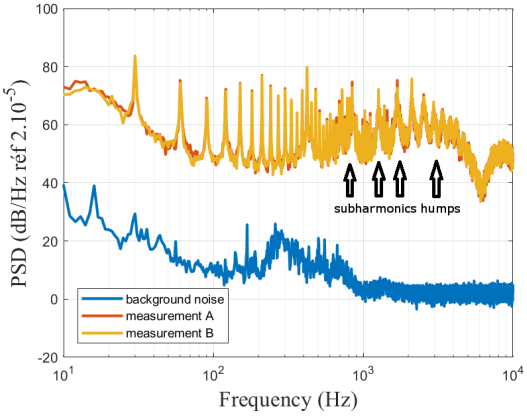

(c) System without front grill and volute

Figure 4: PSD of the far field pressure in front of the fan system ($\Theta = 0°$) and at 3660 RPM (full speed)

Note that the repeatability of the measurements and the associated background is also shown in Fig. 4 for all tested configurations at $\Theta = 0\ °$. Similar results are found on the other microphones of the directivity microphone array. Very low background noise is measured for all configurations. Similar excellent noise results in this new anechoic wind tunnel was recently reported by Padois *et al.* when measuring low trailing-edge noise from controlled-diffusion airfoils [1]. Excellent repeatability is obtained on the broadband noise (maximum variation of 0.5 dB) and a good one on the tonal noise (maximum variations of 2-3 dB). It should be stressed this is typical of other low-speed fans [6].

Directivities

Figures 5 are directivity measurements done at full speed for all configurations. It consists in measuring the sound pressure level vs the radiation angle Θ in decibels (see Fig. 2). In Fig. 5 (a) the OverAll Sound Pressure Level (OASPL) obtained by integrating over the whole frequency range is clearly reduced when both the volute and the front grill are removed from the system as already seen in Fig. 4. An overall 5 to 6 dB noise reduction can be measured. The dominant source also seems to be dipolar as a difference close to 10 dB exists between the front OASPL measured at $\Theta = 0\ °$ and the lateral OASPL at $\Theta = 90\ °$ (in the plane of rotation). Figures 5 (b), (c) and (d) show the directivity plots for chosen BPF harmonics. They do not show as clearly a dipolar behaviour as the OASPL. Yet, the number of lobes increases with the frequency and there is clearly a direction with larger OASPLs per-

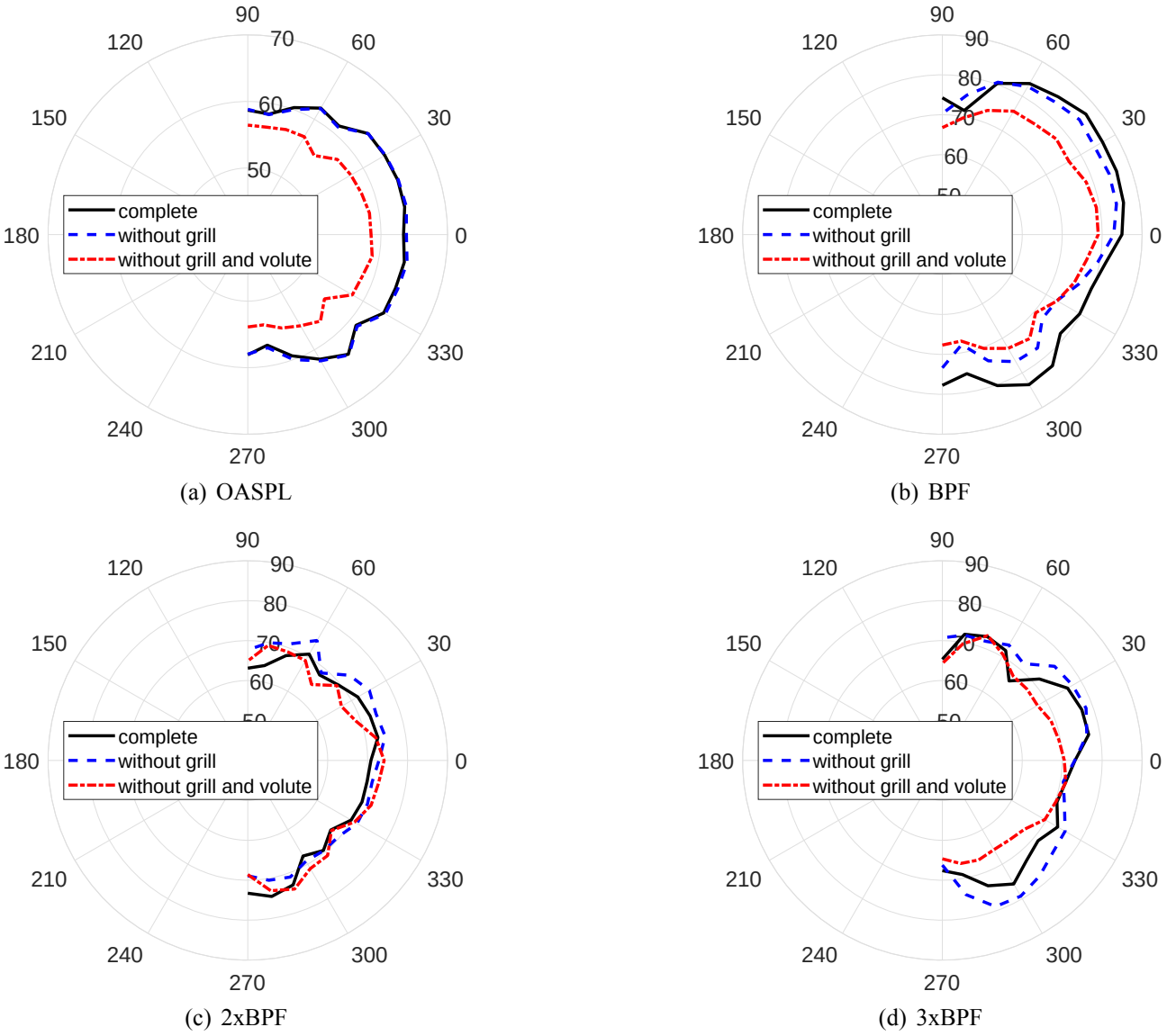

(a) OASPL (b) BPF

(c) 2xBPF (d) 3xBPF

Figure 5: Sound directivity (dB) at 3660 RPM (full speed)

pendicular to a direction with lower OASPLs as expected from a dipole. Two reasons can be evoked for the distorted dipolar directivity. On the one hand, some masking and diffraction can be attributed to the fan environment (support, protection grills and volute) as was already shown by Roger *et al.* in an engine cooling fan module [7, 8] or more recently by Roger and Kucukcoskun in an advanced helicopter tail-rotor configuration [9]. This effect is clearly evidenced at 3BPF when the volute is removed: the additional lobes disappear. On the other hand, as the BPF harmonics are also harmonics of the engine, the behaviour of the acoustic radiation has also a monopolar component. This is evidenced at idle speed where the SPL is much more monopolar and dominated by the engine. For both BPF and 3BPF the reduction of the noise levels is again more important when the front grill and the volute are removed (up to 10 dB reduction). Only the 2BPF noise levels are hardly changed by removing upstream and downstream obstacles: this could mean that this second harmonics is essentially a fan source most likely caused by the tip flow (its mean distortion). Similar results are obtained for the other engine regimes.

For these directivity plots, excellent repeatability is again obtained on the broadband noise (maximum variation of 0.5 dB) and a good one on the tonal noise (maximum variations of 2-3 dB), which confirms

what was observed at $\Theta = 0\,^\circ$ in Fig. 4. Scaling laws of the power spectral densities of the far-field acoustic pressure with fan speed can then be deduced.

Scaling laws

The PSD of all the sources, can be scaled by powers n of the RPM of the fan (or equivalently its rotational speed Ω or its tip speed). Figure 6 presents the scaling done on the noise levels for the three configurations in front of the fan ($\Theta = 0\,^\circ$), at all rotational speeds, as a function of the Strouhal defined as $St = \frac{f}{\mathrm{BPF}}$ based on the blade passing frequency. Similar collapse is observed for all radiation angles.

In such a scaling, the power n of the RPM was taken as 6. The conclusion of this scaling is that the broadband noise can be compared between all measurements in a range of 5 dB and even less beyond $St = 1.5$. This means that the broadband noise is radiating from dipolar sources. Similar collapse is found for the fan BPF harmonics with the same conclusion. However engine orders are not collapsing with this scaling: it is rather found around $n = 4$ which corresponds to a monopole source. Moreover as the engine is hardly producing any broadband noise, we can conclude that the measured broadband noise is produced by the fan system itself as was found in previous low-speed fan studies [10, 5, 11]. This noise is again the lowest in the configuration where the front grill and the volute are removed.

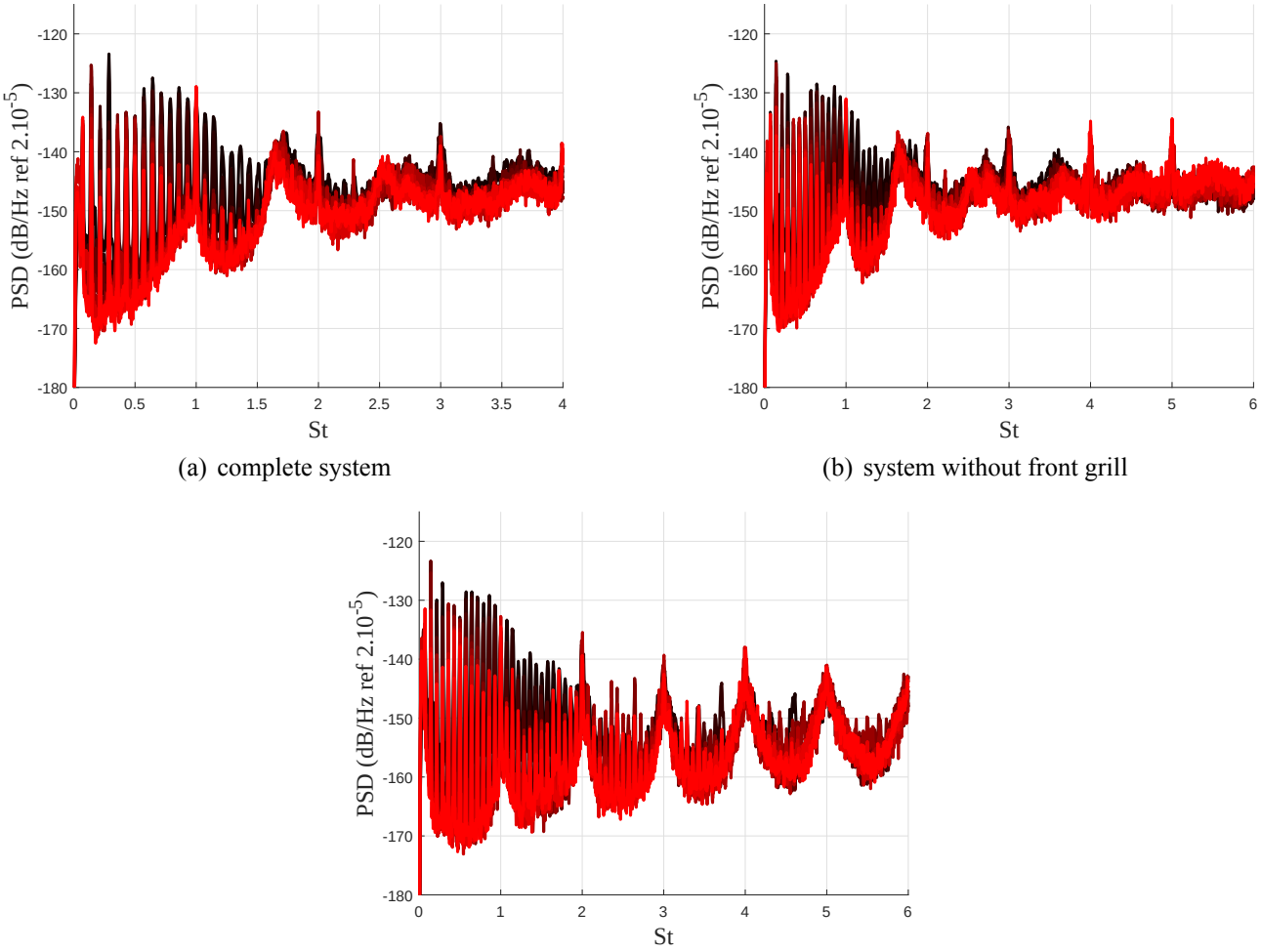

(a) complete system

(b) system without front grill

(c) system without front grill and volute

Figure 6: Scaling with n=6 of PSD measurements for the 3 configurations, in front of the fan system ($\Theta = 0°$).

SEPARATION OF NOISE SOURCES AND TRANSFER PATH

Characterization of the noise source

The next step is to separate both sources contributions in the spectra of figs. 4 and 6.

As the dipolar noise is found to be dominant in the previous section, which conforms with the scaling laws of low-speed fans [11], this sound source can be described by a distributed source force $\nabla \cdot \mathbf{F}$. From Goldstein [12], the acoustic pressure p at an observer position $\mathbf{r}$ is then given by the integral over the source volume V:

$$p(\mathbf{r}) = \iiint_V \left[-\nabla_0 \cdot \mathbf{F}\right]\, g(\mathbf{r}, \mathbf{r}_0)\, dV_0 \tag{1}$$

The subscript 0 denotes a derivative with respect to the source coordinates. An integration by parts yields:

$$p(\mathbf{r}) = \iiint_V \mathbf{F} \cdot \nabla_0 g(\mathbf{r}, \mathbf{r}_0)\, dV_0 \tag{2}$$

If the source is enough compact (Helmholtz number $k\,|\mathbf{r_0}| \ll 1$ with k the acoustic wave number), the Green's function can be separated in near and far field contributions (g_{near} and g_{fs} respectively):

$$g(\mathbf{r}, \mathbf{r}_0) = \chi(\mathbf{r})\, g_{fs}(\mathbf{r}, \mathbf{r}_0)\, g_{near}(\mathbf{r}_0) \tag{3}$$

with

$$g_{fs}(\mathbf{r}, \mathbf{r}_0) = \frac{e^{ik|\mathbf{r}-\mathbf{r}_0|}}{4\pi|\mathbf{r}-\mathbf{r}_0|} \qquad \text{and} \qquad \nabla_0 g_{fs}(\mathbf{r}, \mathbf{r}_0) \approx ik\, g_{fs}(\mathbf{r}, \mathbf{r}_0)\, \frac{\mathbf{r}_0}{|\mathbf{r}_0|} \tag{4}$$

the free field Green's function and its gradient in the far-field ($k\|\mathbf{r}\| \ll \mathbf{1}$); $g_{near}(\mathbf{r}_0)$ is a dimensionless Green's function characterizing near-field effects such as Doppler shifts due to moving sources, geometrical non-compactness, and other effects due to both propagating and nonpropagating components and χ a coefficient taking into account amplification and attenuations coming from boundary conditions (caused by the fan installation: the volute, the front and back grills…). Then the acoustic pressure becomes in the far field

$$p(\mathbf{r}) = ik\, \chi(\mathbf{r})\, g_{fs}(\mathbf{r}) \iiint_V \mathbf{F} \cdot \frac{\mathbf{r}_0}{|\mathbf{r}_0|} \left[g_{near}(\mathbf{r}_0) + \frac{\nabla_0 g_{near}(\mathbf{r}_0)}{ik}\right] dV_0 \tag{5}$$

This is a generalization of Stephens' result for any dipolar force orientation (Eq.(13) in [10]). The autospectrum of the far-field acoustic pressure $\mathcal{P}$ at a point $\mathbf{r}$ in the far field of a fan is then

$$\begin{aligned}\mathcal{P} =& |\chi(\mathbf{r})|^2 k^2 |g_{fs}(\mathbf{r})|^2 \iiint_{V_1} \cdot \iiint_{V_2} \overline{F_{r_1} F^{\star}_{r_2}} \\ &\times \left[g_{near}(\mathbf{r}_{01}) + \frac{\nabla_{01} g_{near}(\mathbf{r}_{01})}{ik}\right] \left[g_{near}(\mathbf{r}_{02}) + \frac{\nabla_{02} g_{near}(\mathbf{r}_{02})}{ik}\right]^{\star} dV_{01} dV_{02}\end{aligned} \tag{6}$$

with F_r the projection of the force $\mathbf{F}$ in the $\mathbf{r}$ direction. Consequently, $\mathcal{P}$ is given by the product [10]:

$$\mathcal{P} = \mathcal{F} \cdot \mathcal{T} \tag{7}$$

where $\mathcal{F}$ and $\mathcal{T}$ are respectively a force function depending on sources located at $\mathbf{r}_0$ onto the fan and a transfer path function from the source to the receiver located at $\mathbf{r}$. The transfer path function $\mathcal{T}$ is then

$$\mathcal{T} = |\chi(\mathbf{r})|^2 k^2 |g_{fs}(\mathbf{r})|^2 \tag{8}$$

It does not depend on the dipole forces. Note that if an axial dipole is considered, $F_r = F \cos\theta$ and the expression given in [10] is recovered by transfering the $\cos^2\theta$ in the transfer function.

Source separation

As in [10] let's assume that a function $\mathcal{F}_0$ exists such that

$$\begin{aligned}\mathcal{F} = &\iiint_{V_1} \cdot \iiint_{V_2} \overline{F_{r_1} F^{\star}_{r_2}} \\ &\times \left[g_{near}(\mathbf{r}_{01}) + \frac{\nabla_{01} g_{near}(\mathbf{r}_{01})}{ik} \right] \left[g_{near}(\mathbf{r}_{02}) + \frac{\nabla_{02} g_{near}(\mathbf{r}_{02})}{ik} \right]^{\star} dV_{01} dV_{02} \\ &= \mathcal{F}_0(St) M_{tip}^{n(St)}\end{aligned} \tag{9}$$

with M_{tip} the tip Mach number so that:

$$\log(\mathcal{F}) = \log(\mathcal{F}_0(St)) + n(St) \cdot \log(M_{tip}) \tag{10}$$

According to this expression, at each value of St, a plot of $\log(\mathcal{F})$ vs. $\log(M_{tip})$ should be a straight line with slope $n(St)$. The function $\mathcal{F}_0(St)$ is based on Strouhal number, can be seen to be determined by the motion of the impeller, and to describe the spectral distribution of the aerodynamic sound generated inside the fan.

Consequently the logarithm of $\mathcal{P}$ can be written as :

$$\log(\mathcal{P}) = \log(\mathcal{F}_0) + n \cdot \log(M_{tip}) + \log(k^2) + \log(|g_{fs}|^2) + log(|\chi|^2) \tag{11}$$

In this expression $\mathcal{F}_0$, n and χ are unknown. The source separation algorithm seeks to find the function χ that, in a least squares sense, best fits this expression given measurements of $\mathcal{P}$ at several values of M_{tip}. [10]

The coefficient n is usually between 5 and 6 for a typical axial dipole sources related to blade loads [13]. This is confirmed by the scaling laws shown above for the present fan system. This means that scaling the Power Spectrum level by M_{tip}^n should result in a superposition of the level for all contents related to dipole forces implied in the acoustic radiation process. For sake of simplification, as the M_{tip} is related to the RPM of the engine, the scaling will be done using Ω^n.

As mentioned above, a series of measurements have been done at several RPM from idle to maximum speed which enables to separate the contribution of dipolar force sources. Using the above scaling method, it will be easy to separate the contribution of dipole sources forces from all the other sources coming especially from the engine itself (which are mostly not related to dipole type of force source as already shown above).

Results

Figure 7 shows the result of the noise-source separation algorithm [10] presented in the previous section. Figure 7 (a) shows the function $|\chi|^2$ that stands for the effects of the boundaries in Eqs. (3), (8) and (11). This function is revealing an installation effect in the frequency range of 6 kHz. This is most likely caused by the reflection or diffraction of acoustic waves on the fan module (wavelength similar to the volute depth for instance). In Fig. 7 (b) the coefficient n is between 5 and 6 at relatively high frequencies where the engine is not radiating any noise. This is confirming the acoustic dipolar behavior of blade loads. At low frequencies, the behavior is more of a monopole. In Fig. 7 (c), the SPL measurement and the estimation of blade loads radiation have been plotted. The estimation of blade loads contributions no longer include the 15 dB fluctuation at 6 kHz, mostly caused by the diffraction on the engine and/or the volute. The conclusion is the same for all configurations tested. As was

already found by Stephens and Morris, a smooth decay towards high frequencies is now observed on the fan spectrum [10].

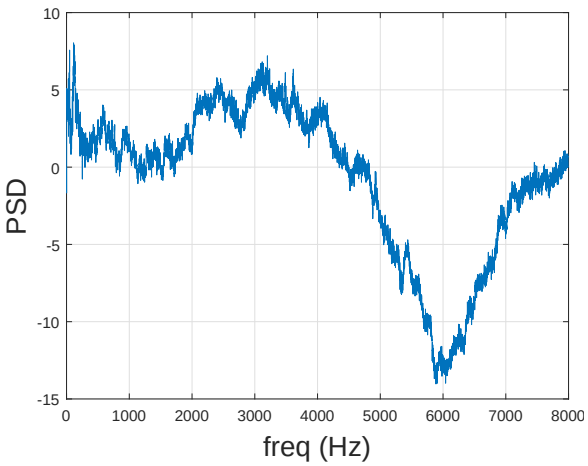

(a) $|\chi|^2$ vs frequency

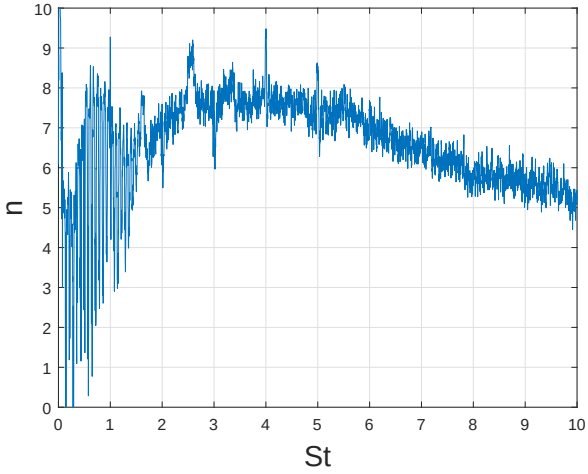

(b) n vs Strouhal

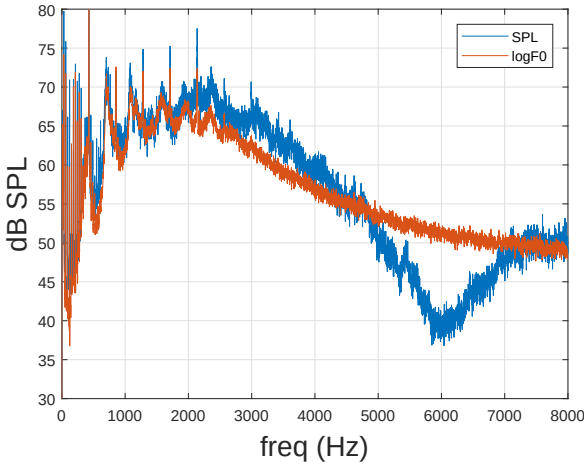

(c) SPL measured at $\Theta = 0°$, and estimation of $\mathcal{F}_0$ at full speed

Figure 7: Noise-source identification using the separation algorithm for the complete system

CONCLUSIONS AND PERSPECTIVES

In the present study the acoustic characterization of a smoke-removal fan system has been achieved. Three different configurations have been studied at various engine regimes. Two main noise sources have been identified in all configurations of this fan system: one at lower frequencies that corresponds to the thermic engine and one at mid to high frequencies that corresponds to the fan and its interaction with its environment. The former is monopolar while the later is rather dipolar. The engine is louder than the fan itself at low speeds while both sources contribute equally at full speed. The main noise features of this fan system are a dipolar broadband noise, and a mixed monopolar and dipolar tonal noise at engine orders and at the BPF and its harmonics respectively. At full speed, the OASPL exhibit a dipolar directivity, while the pattern at the tonal frequencies multiple of the BPF was less clearly dipolar. This is caused by the possible installation effects and diffraction of the fan noise on its environment, and by the fact that all BPF frequencies are harmonics of the thermic engine itself.

Nevertheless, the broadband noise component nicely follows the power law that characterizes dipolar acoustic radiation (power 6 at low frequencies and power 5 at high frequencies). Finally the noise source separation proposed by Stephens and Morris has been succesfully extended and applied to the present system [10]. Some of the installation effects can then be removed from the fan spectra at high frequencies.

Among the different tested configurations, the best reduction in terms of SPL is observed when removing the front grill and the volute. Almost no difference is seen when removing the grill alone, which stresses that wake interaction and potential from this obstacle is negligible. The tip clearance is kept large enough on this fan for security reason. This is most likely the main cause of broadband noise as evidenced by the large subharmonic humps that are seen in all configurations. When the volute is present this is an additional main contributor to the overall broadband noise. Tonal noise is more difficult to control. In fact, only removing the front grill to minimize the interaction between the blades and fixed parts, does not reduce the noise level significantly. Removing the volute provides up to 10 dB reduction but only on the first and third BPF and mostly on the latter, which suggests that the volute provides some strong noise diffraction. The second BPF is not affected by the upstream and downstream obstacles, and is mostly caused by the tip clearance flow. Moreover, the flow is strongly perturbed by the engine itself and surely contributes to the strong tonal noise seen in all configurations.

The perspective for some noise reduction can therefore be foreseen in some passive way to cancel the sound source due to inflow inhomogeneousity. For instance a particular circumferential obstruction pattern as suggested by A. Gérard *et al.* [14] could be used, which can give some reduction up to 9 dB on the BPF and its harmonics. The same technique has also been successfully applied to centrifugal fans [15]. A more costly alternative is to consider active noise control with some dipolar acoustic transducer mounted at the center of the front fan grill that cancels the acoustic dipolar radiation of the fan system for instance [16]. The similarity of radiation patterns gives some good results also on BPF and may be used for the broadband noise as well. Efficient and selective control algorithm as recently proposed by Pasco *et al.* could also be used [17].

REFERENCES

[1] T. Padois, P. Laffay, A. Idier, and S. Moreau. *Detailed experimental investigation of the aeroacoustic field around a Controlled-Diffusion airfoil*. In *21st AIAA/CEAS Aeroacoustics Conference*, page 2205, **2015**.

[2] M. Roger, S. Moreau, and A. Guedel. *Broadband Fan Noise Prediction using Single-Airfoil Theory*. Noise Control Eng. J., 54(1):5–14, **2006**.

[3] M. Roger and S. Moreau. *Extensions and limitations of analytical airfoil broadband noise models*. Int. J. Aeroacoust., 9(3):273–305, **2010**.

[4] S. Moreau and M. Roger. *Competing Broadband Noise Mechanisms in low-speed axial fans*. AIAA J., 45(1):48–57, **2007**.

[5] S. Moreau and M. Sanjosé. *Sub-harmonic broadband humps and tip noise in low-speed ring fans*. J. Acoust. Soc. Am., 139(1):118–127, **2016**.

[6] D. Casalino, S. Moreau, and M. Roger. *One, no one and one hundred thousand methods for low-speed fan noise prediction*. Int. J. Aeroacoust., 9(3):307–327, **2010**.

[7] M. Roger and S. Moreau. *Aeroacoustic installation effects in cooling fan systems. Part. 1: Scattering by surrounding surfaces*. In *12th International Symposium on Transport Phenomena and Dynamics of Rotating Machinery*, March **2008**.

[8] S. Moreau, O. Marck, and M. Roger. *Aeroacoustic installation effects in cooling fan systems. Part. 2: Near-field and ground effects*. In *12th International Symposium on Transport Phenomena and Dynamics of Rotating Machinery*, March **2008**.

[9] M. Roger and K. Kucukcoskun. *Near and far field modeling of advanced tail-rotor noise using source-mode expansions* . In *17th International Symposium on Transport Phenomena and Dynamics of Rotating Machinery*, March **2017**.

[10] D.B. Stephens and S.C. Morris. *A method for quantifying the acoustic transfer function of a ducted rotor*. J. Sound Vib., 313:97–112, **2008**.

[11] Alain Guédel. *Acoustique des ventilateurs*. Éditions PYC livres, **1999**.

[12] M. Goldstein. *Aeroacoustics*. McGraw-Hill, **1976**.

[13] T. J. Mueller. *Aeroacoustic Measurements*. **2001**.

[14] A. Gérard, A. Berry, P. Masson, and Y. Gervais. *Experimental validation of tonal noise control from subsonic axial fans using flow control obstructions*. J. Sound Vib., 321:8–25, **2009**.

[15] A. Gérard, M. Besombes, A. Berry, P. Masson, and S. Moreau. *Tonal noise control from centrifugal fans using flow control obstructions*. Noise Control Eng. J., 61(4):381–388, **2013**.

[16] A. Gérard, A. Berry, and P. Masson. *Control of tonal noise from subsonic axial fan. Part 2: Active control simulations and experiments in free field*. J. Sound Vib., 288(4):1077–1104, **2005**.

[17] Y. Pasco, P.A. Gauthier, and A. Berry and. S. Moreau. *Interior sound field control using generalized singular value decomposition in the frequency domain*. J. Acoust. Soc. Am., 141:33–345, **2017**.

ACKNOWLEDGEMENTS

The authors gratefully acknowledge the funding by NSERC on the Engage grant number EGP 47646514.